ADVANCED FUNCTIONAL MATERIALS
www.afm-journal.de

Metastable Liquid–Liquid Phase Separation and Aging Lead to Strong Processing Path Dependence in Mini-Spidroin Solutions

*Dmitrii Fedorov, Fred-Eric Sammalisto, Adam L. Harmat, Martin Ahlberg, Salla Koskela, Mikko P. Haataja, Alberto Scacchi, Maria Sammalkorpi, and Markus B. Linder**

Recombinant silk proteins provide a route toward sustainable and biocompatible materials. For making such materials, the assembly process from dilute protein into a functional material is central. The assembly mechanism in engineered materials is by necessity different from the natural ones—this poses challenges but also opens opportunities for scaling up and for developing novel properties. The phase behavior of a mini-spidroin, NT-2Rep-CT is studied, which is a widely studied variant of recombinant silk. NT-2Rep-CT can be triggered to assemble by lowering the pH, but even at high pH—considered as storage conditions—it can be in various states, such as forming condensates, clusters, gels, and soluble protein. It is shown how its assembly phases evolve through both metastable and dynamically arrested states. The observed behavior of silk protein solutions is highly complex, and elements thereof from phase diagrams associated with polymers, colloidal systems, and globular proteins are found. Based on the characterization of cluster formation and structural intermediates, a minimalist phase diagram is proposed for NT-2Rep-CT and argues that the understanding and insight into silk assembly via its phase behavior, and especially the arrested states, is central for designing recombinant silk proteins and their processing for materials applications.

1. Introduction

Silk is one of the most studied biomimetic models for materials and biosynthetic silk holds much potential as a sustainable material for a wide range of applications.[1] Spider silks in particular have impressive properties that have received much attention for understanding and mimicking. They form a family of sequences and have different repetitive motives depending on their origin.[2] Spider silks, or spidroins—with dragline silks as the main model—contain hydrophobic alanine repeats that are initially α-helical or adopt a random coil secondary structure. These undergo structural transitions into β sheets which form crystallites that interconnect silk protein molecules.[3,4] These long and repetitive sequences are initially not folded into defined structures but are in their soluble state disordered. Such proteins are termed intrinsically disordered proteins

D. Fedorov, F.-E. Sammalisto, M. Ahlberg, S. Koskela, A. Scacchi, M. B. Linder
Department of Bioproducts and Biosystems
Aalto University
P.O. Box 16100 Aalto, Espoo 00076, Finland
E-mail: markus.linder@aalto.fi

D. Fedorov, F.-E. Sammalisto, A. L. Harmat, M. Ahlberg, S. Koskela, A. Scacchi, M. Sammalkorpi, M. B. Linder
Center of Excellence in Life-Inspired Hybrid Materials (LIBER)
Aalto University
P.O. Box 16100 Aalto, Espoo 00076, Finland

A. L. Harmat, M. Sammalkorpi
Department of Chemistry and Materials Science
Aalto University
P.O. Box 16100 Aalto, Espoo 00076, Finland

The ORCID identification number(s) for the author(s) of this article can be found under https://doi.org/10.1002/adfm.202410421

M. P. Haataja
Department of Mechanical and Aerospace Engineering
Princeton University
Princeton, NJ 08544, USA

M. P. Haataja
Omenn-Darling Bioengineering Institute
Princeton University
Princeton, NJ 08544, USA

A. Scacchi
Department of Applied Physics
Aalto University
P.O. Box 11000 Aalto, Espoo FI-00076, Finland

A. Scacchi
Department of Mechanical and Materials Engineering
University of Turku
Turku 20014, Finland

DOI: 10.1002/adfm.202410421

(IDP) or are said to contain intrinsically disordered sequences or regions (IDR).[5]

Recombinant production of silk proteins opens possibilities to industrially produce silk materials in a scalable way.[6] The challenge has been to understand how the silk proteins can be assembled into a material using industrially compatible processes. For designing such proteins, the structural engineering of silk proteins should be carried out in synchrony with process development so that an optimal process is obtained. In such a process the structural features of the protein optimally fit the assembly steps during processing and also result in an excellent material.[1] A breakthrough was reached when it was understood that the N-terminal domain of spider silk is a folded domain functioning as a pH switch that is monomeric at pH above 7, and forms a dimer at pH 5.[7] The silk proteins also contain C-terminal domains that are dimeric under most conditions.[8] The basic unit of silk proteins are therefore dimers through their C-termini, and can be switched by a lowering of pH to become—in principle infinitely long—multimeric chains. This understanding has resulted in processing designs where a soluble silk dope is kept at a pH above 7 and then extruded as a filament into a coagulation bath with a pH of 5. Typically, the starting buffer for the silk dope has been a 20 mM Tris buffer at pH 8.0.[9] During assembly, it has been observed that the C-terminal domain is not only functioning as a passive dimerizing unit but undergoes complex structural transitions resulting in β-sheet conformations that are linked to solidification mechanisms.[8,10,11] By making a smaller engineered variant—called a mini-spidroin—that has functional N- and C-terminal domains, but only two repetitive sequence units, an efficient assembly protocol could be established.[11] The engineered mini-spidroin variant was named NT-2Rep-CT, according to its structure. The short repetitive units gave excellent production yields and good processing properties for the spinning dope.[12] Silk proteins not only undergo transitions into filaments but also gels. For example, the NT-2Rep-CT was heated to 37 °C, which resulted in a strong hydrogel.[13] Surprisingly even NT itself could form a gel when heated.[13]

Wider studies of silk proteins have led to the conclusion that it is not only the terminal domain dimerization that is important for their molecular assembly process. Especially the occurrence of phase transitions, such as liquid–liquid phase separation (LLPS), forming intermediate states between soluble protein and final material, has received much attention.[14,15] LLPS is a phase transition where a protein solution forms a coexistence of high- and low-density liquid phases. The protein-rich droplets, often referred to as biomolecular condensates, biocondensates, or coacervates in the literature, are thought to preassemble silk proteins, and it was found that pulling fibers from silk solutions was strongly enhanced if the dope had undergone LLPS.[16] Also functions such as adhesiveness have been shown to be strongly enhanced.[17] More widely, phase transitions involving proteins are receiving much attention as a research topic.[18,19] On the one hand, other research on the assembly of biological materials also highlights the importance of LLPS as a pre-assembly step in materials formation.[20] These studies include examples such as marine adhesives, squid beak proteins, and elastin.[21–23] On the other hand, in cell biology phase transitions take part in a large variety of cellular processes, such as during cell development and in response to stress.[24–27]

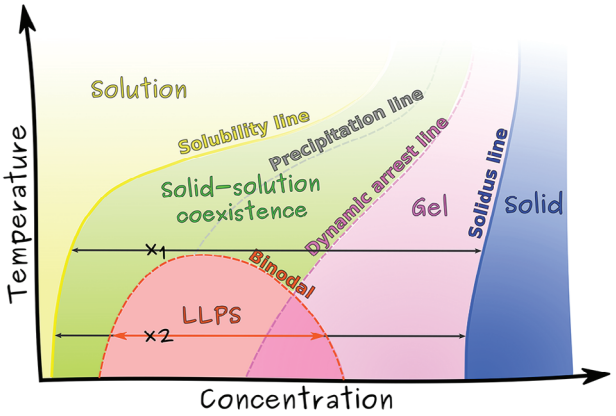

Figure 1. Schematic illustration of a state diagram for globular protein solutions assuming the interactions and secondary structure do not change with temperature. Replacing temperature in the y-axis by inverse attraction strengths allows for higher generalizability, see, e.g., McManus et al.[31] The continuous lines represent phase boundaries (three equilibrium phases: solution, solid-solution coexistence, and solid), while the dashed lines mark regions (metastable solution, LLPS, gel) where intermediate states may form. The precipitation line indicates where the solution becomes unstable and spontaneously forms a solid. The presence and location of the depicted states are not universal for all proteins and depend on solution conditions. Points x1 and x2 represent different compositions that evolve into different co-existence phases. Refs. [28,31,48,53] provide a more extensive discussion.

Given the importance of LLPS in biological processes, several attempts to construct a unified framework for describing protein solution phase transitions exist.[28–33] For miscible solution species, the two-phase co-existence region arises when the effective interactions between the solution species are stronger than a critical interaction strength, resulting in a miscibility gap. The two liquid phases are characterized by equal pressures and chemical potentials. This picture is considered, e.g., in polymer physics approaches adopted for describing solutions and assembly phases of IDPs.[5,34–36] However, in vitro experiments have shown that over time, protein solutions of IDPs exhibiting co-existing phases may form solid-like aggregates or other assembly structures,[37–39] suggesting that the original coexistence is not a thermodynamic equilibrium state, but rather a metastable one.[33–35,40] This metastability of the coexistence region is in fact well-established for globular protein solutions.[31] For example, complete temperature-concentration phase diagrams demonstrating the metastable character of several assembly phases, including the liquid–liquid co-existence phase, exist for several globular proteins such as γ-Crystallin[41–44] and lysozyme.[45] This variety of assembly states in globular protein solutions is presented in **Figure 1**, where an idealized schematic of the assembly phases for a globular protein solution is shown. We note that the assembly response in such protein solutions bears close resemblance to colloidal phase diagrams.[28,41] Now, in a colloid phase diagram, and in the globular protein picture, the solution, solid-solution co-existence, and solid regions are equilibrium phases. The coexistence region associated with LLPS in colloids and globular protein solutions is a metastable state within the equilibrium solid-solution coexistence region, which may persist over experimentally relevant timescales (up to

several hours).[46–48] Such metastability has been shown to arise from the presence of short-range attractive interactions relative to their size.[41,49,50] Due to the potentially slow transient nature of LLPS (several hours) compared to the typical experimental characterization time (minutes), the observed response can resemble the one predicted by an equilibrium two-phase coexistence state. Thus, it is not surprising that the equilibrium two-phase model is often invoked to describe liquid–liquid coexistence. However, the presence of long-range interactions, i.e., electrostatics, or the addition of IDPs are known to increase the diversity of obtainable assembly states.[28] Specifically, the mini-spidroins here, consisting of multiple domains including IDPs and globular domains, are hence likely to exhibit an assembly response more complex than those associated with globular proteins. The increased complexity in the assembly also gives rise to dynamically arrested nonequilibrium states.

Here we investigate the phase behavior of the mini-spidroin NT-2Rep-CT. To understand the assembly of NT-2Rep-CT into various forms of materials, a critical step is to unravel the relation between self-assembly and the underlying phase diagram. Recently, the formation of condensates of mini-spidroins has been observed, and connections to materials formation have been suggested. LLPS is strongly promoted in buffers such as phosphate and ammonium acetate.[51,52] A thorough understanding is not only needed for the wider theme of protein-based materials, but such well-defined artificial systems can also shed light on the fundamental processes in cells, where biological materials naturally form. To this end, we have carried out an extensive experimental characterization effort to probe the temporal evolution of NT-2Rep-CT solutions over a wide range of temperatures, solution pH conditions, and protein concentrations. We have observed simple uniform solutions in dilute systems, the presence of metastable liquid–liquid coexistence, and the emergence of irreversible aggregates at higher concentrations. Perhaps most importantly, our experiments highlight the critical role of aging on the final state of the protein solution. Finally, based on our experimental observations, we construct a minimalist phase diagram for NT-2Rep-CT and highlight its salient features vis-a-vis colloidal/globular protein systems.

2. Results and Discussion

2.1. Clusters of NT-2Rep-CT are Widely Observed at pH 8 at 20 °C

The state of NT-2Rep-CT at 20 g L^{-1} in the spinning starting buffer—20 mM Tris at pH 8.0—was first analyzed by analytical ultracentrifugation (AUC). In this condition NT is monomeric, and this buffer is frequently used when preparing spinning dopes. Analysis of the distribution of the sedimentation coefficient, $c(s)$, revealed the presence, along with NT-2Rep-CT dimers, of a significant amount of very high molecular weight assemblies. In this work, we call these assemblies that have a varying number of NT-2Rep-CT monomer, clusters. The protein clusters in this work can be dynamic or arrested in nature. More specifically, **Figure 2A** shows that the molecular weights of clusters reached up to tens of MDa. The peak at $s = 4$ S is identified as the NT-2Rep-CT dimer peak, indicating that the clusters contain well over 500 dimer units for $s = 300$ S ($f/f_0 = 1.5$). The overall fraction of high molecular weight clusters in the range of sedimentation coefficient from 10 to 500 S corresponds to ≈40% of the total signal. Previous studies using mass spectrometry initially demonstrated that NT-2Rep-CT produces clusters larger than the expected dimers, forming structures up to octamers, although measurements were done at different buffer and pH conditions—not in the spinning starting buffer as here.[14,54] By AUC, both the fraction of molecules as clusters and the molecular weight of the clusters were much larger than the previously applied mass spectrometry technique allowed for observation. The ability of AUC to detect large structures is enhanced by its minimal perturbation to the system, as it does not require ionization or other interference with the sample itself.

2.2. NT-2Rep-CT solution is metastable and undergoes dynamic arrest while storing at pH 8, 20 °C

In the model phase diagram, as shown in Figure 1, a metastable solution can exist between the solubility and precipitation lines, and metastable liquid–liquid coexistence can also be observed in the experimental observation timescale. Furthermore, the solid-solution coexistence region can become dynamically arrested and evolve to form a gel. To investigate NT-2Rep-CT solution in terms of the model phase diagram under storage buffer conditions (20 g L^{-1} NT-2Rep-CT at pH 8, 20 mM Tris), the changes over time in the fraction of higher order clusters present in the solution were quantified using AUC. An increase in these clusters infers metastability of the protein solutions.[55] To this purpose, we performed the AUC measurements at different times 0, 18, 48, and 120 h, with time 0 meaning directly after thawing the stock sample. At time 0 the protein solution was clear by visual and microscope inspection. Figure 2B shows primary AUC sedimentation velocity data demonstrating qualitatively that cluster formation increases markedly in the protein solution over the time interval studied, i.e., up to 120 h. The strong decrease in signal intensity shows that a large portion of protein clusters with rapid sedimentation so that the overall signal (protein content) decreases to 20% over the time interval (Figure 2C). Simultaneously the proportion of the signal from the smallest unit—NT-2Rep-CT dimer—in solution decreases from ≈45% to 10% of the original concentration in a continuous manner over 120 h (Figure 2D). Corresponding samples were studied visually (Figure 2B). At the protein concentration of 40 g L^{-1} the solution was liquid for up to ≈120 h (at 20 °C) and then formed a gel. The transition from liquid to gel was determined by vial inversion tests. The observation that clusters grow over time suggests that the protein solution is metastable in relation to solid-solution coexistence, however, the solution can also form dynamically arrested states as it evolves in time, see Figure 1. In the schematic phase diagram, this means that the 40 g L^{-1} NT-2Rep-CT pH 8.0 Tris 20 mM solution is in the vicinity of state point x_1. While evolving toward solid-solution coexistence, the kinetic path of the system is such that the local concentration surpasses the concentration threshold for gelation, thus triggering its formation. To further probe the mechanisms of NT-2Rep-CT gelation and to understand the kinetics of this transition, we performed a set of experiments at increasing temperatures, 20, 25, 30, and 37 °C to study the time until gelation. We found that the time until gelation decreased

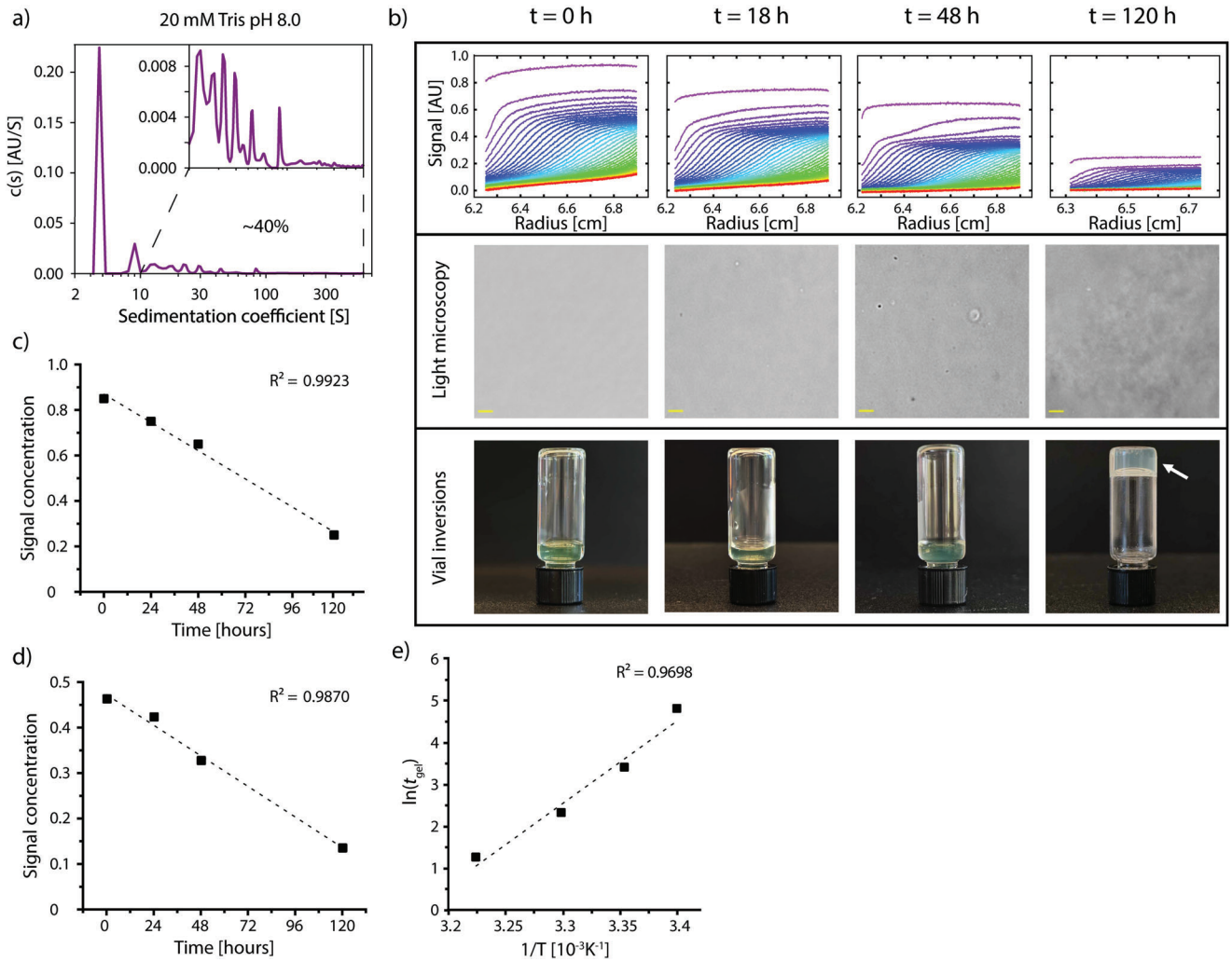

Figure 2. The phase behavior of NT-2Rep-CT at pH 8.0. A) Sedimentation velocity experiments show that NT-2Rep-CT forms large clusters of over 300 S at pH 8.0 in 20 mM Tris buffer. The dimer peak at 4 S is prominent. B) Sedimentation velocity curves from overtime for pH 8.0 samples that were stored at 20 °C after thawing for 0, 18, 48, and 120 h. The initial curve (magenta, uppermost) is at 2 min after starting the AUC experiment and the last data collection curve (lowermost, red) was at time 700 min. The more rapid decrease of signal for samples stored longer shows an increase in clustering in the sample. Samples were inspected visually by light microscopy. Scale bar 20 µm. The time point of gelation was determined by vial inversion tests. C) The increase of large clusters is such that the proportion of soluble protein (detection signal) that is not immediately sedimented decreases from 90% to 20% over 120 h. D) The fraction of NT-2Rep-CT in the dimer form in solution decreases from ≈45% to 10% over 120 h. E) Arrhenius plot over the temperature dependence for gel-formation.

with increasing temperature. Plotting the data according to a linearization of the Arrhenius law we found a good fit and an activation energy toward gelling of 164 kJ mol^{-1} (Figure 2E). This value is consistent with protein studies where the activation energy was associated with secondary structure change.[56–58] We note that the Arrhenius response here implies a fixed effective activation energy toward cluster growth until a percolating system is reached. This points toward the secondary structure change being the rate-limiting step throughout the examined temperature range for gelation.[59] This is consistent with the findings of Arndt et al. where the NT terminal domain secondary structure change was attributed to gelation.[13]

Next, we studied the size and the time dependence of clusters at much lower concentrations. AUC sedimentation velocity experiments were performed for samples containing 0.05, 0.1, 1, 5, and 10 g L^{-1} NT-2Rep-CT in 20 mM Tris pH 8.0. We observed that clusters were smaller overall, and the growth of clusters was suppressed at the lowest concentrations of 0.05–1 g L^{-1} (**Figure 3**; Figure S1, Supporting Information). Meanwhile, number of clusters was growing over time at concentrations of 5 and 10 g L^{-1}. Compared to the model phase diagram (Figure 1), the results are consistent with the solubility line being in the region between 1 and 5 g L^{-1}. To the left of the solubility line, the solution is thermodynamically stable, and cluster growth was not observed. Cluster formation inside the solid-solution coexistence region has been attributed to the formation of pre-nucleation clusters described by classical nucleation theory as well as the formation of mesoscale high-density liquid-like clusters that are considered to be a preassembly step for crystal nucleation.[60] A two-step nucleation mechanism was proposed for the latter case.[60–62] More

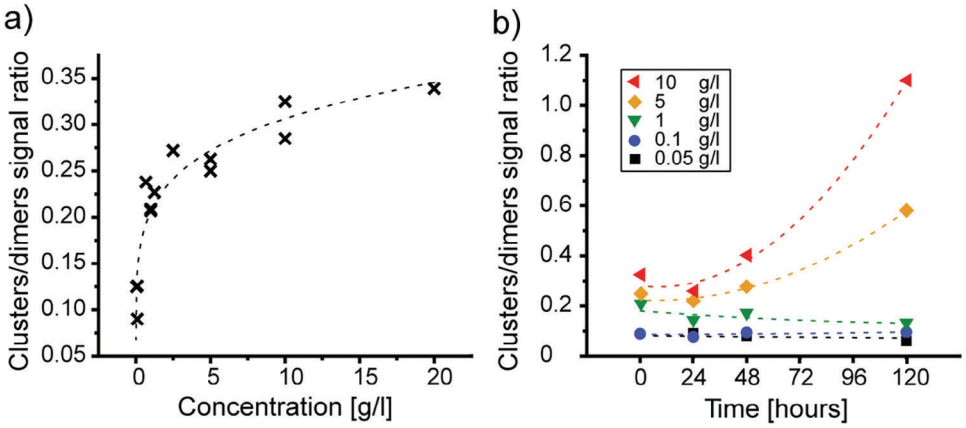

Figure 3. AUC analysis of the effect of dilution on NT-2Rep-CT clusters. A) The ratio of integrated signals from all clusters larger than the dimer to the signal of the dimer for different concentrations of protein as a function of protein concentration. The fraction of molecules in large clusters compared to dimers decreases strongly below 5 g L^{-1}. B) The time evolution of cluster growth is shown as the signal ratio for the clusters larger than the dimer to the dimer. At concentrations of 1 g L^{-1} and under, clusters did not grow, while clusters grew strongly with time at concentrations above 5 g L^{-1}.

recently, clusters have also been observed to the left of the solubility line in the stable undersaturated solution for globular protein,[55] amino-acid,[63] and salt solutions.[64,65] The cluster lifetimes in these undersaturated solutions were shown to be short-living and dynamic, with lifetimes ranging from ms to s.[55,66]

2.3. Altering Phase Behavior by Changing Solution Conditions

By decreasing the solution by 0.8 units to pH 7.2 and increasing the Tris concentration from 20 to 110 mM, we found that the behavior of NT-2Rep-CT mini-spidroin changed markedly. We studied the effect of the pH change in the size distribution of clusters in solution by AUC at 20 °C. At pH 7.2 the NT domain is still monomeric,[7] but our AUC results show a marked increase in clusters over a broad range of sizes, up to over 300 S (**Figure 4A**). The amount of high molecular weight clusters grew by ≈12% by the pH change. Simultaneously, two additional peaks appeared in the range of sedimentation coefficients between 1 and 10 S. The pronounced peak at $s = 6.0$ S corresponds to tetramers while the peak at $s = 8.1$ S, corresponds to hexamers. These two additional peaks accounted for ≈25% of the total signal, and ≈23% of the sample remained in dimeric form. The remaining 52% of the signal were from clusters more than $s = 10$ S. Previous mass spectrometry investigations suggested that the largest clusters at pH 7.5 were traces of tetramers, and even at pH 5.5 only small amounts of octamers were found, with no signal from larger clusters than this.[54]

The samples also changed visually. We observed the formation of condensate droplets instantaneously when the conditions were changed from pH 8.0–pH 7.2 (Figure 4B) at 20 °C. We studied the effect of sample age in two ways, first by letting the pH 8.0 sample age for different times and then making the pH change. Alternatively, we imposed the pH change at time 0 and then allowed the sample to age. In both cases, a strong time dependence was observed. When the pH drop was done at different time points after thawing the pH 8.0 solution, we observed at time 0 liquid-like condensates, at 18 h gel-like condensates, at 48 h irregular assemblies, and at 120 h a gel had already formed in the pH 8 sample which remained even after the pH drop (Figure 4B). We describe condensates as liquid-like if we observed droplets that underwent rapid fusion events, and as gel-like if no fusion events could be observed. Often such gel-like condensates had a rough surface structure. Droplet fusion events were in the timeframe of 1–10 s depending on initial droplet sizes and age (Video S1, Supporting Information). Letting the samples age after the pH drop led to a change in the appearance of the condensates (Figure 4D). The condensates became gel-like and after 120 h the sample still flowed in the vial inversion test and the sample contained irregularly shaped assemblies. If the sample was at 8 °C during pH change in the aging experiments, we found a very different outcome. Condensate droplets formed initially as at 20 °C but over time the droplets remained liquid-like and grew larger (Figure 4E). After 120 h at 8 °C the droplets were still liquid-like, but with increased viscosity (Figure 4F).

Comparing our results to the phase diagram in Figure 1, we note that the data fits with a system where the pH change leads to a shift of the diagram upward so that the initial timepoint lands in a region below the binodal, into a liquid two-phase region. The position would correspond to point x_2 of the phase diagram in Figure 1. The observed changes in the phase diagram point to an increase in protein–protein interactions. This is consistent with previous work where an altered surface charge distribution of the NT domain was attributed to the increased propensity of the protein to form higher-order assemblies, although at a lower pH 6.3.[7] Also, it is important to point out that dynamic arrest resulting in the formation of gel-like condensates, irregularly shaped assemblies or gels happens within experimental observation time (120 h) in all experiments within the solid-solution coexistence region. While the size of these solid-like assemblies varies, from system-spanning gel-like states to finite-sized irregular assemblies, we hypothesize that the structure of the assemblies is comparable and is a consequence of the dynamics being restricted on a short timescale. Therefore, the pathway to equilibrium can be so long that it becomes unobservable in experimental observation timescale. This makes these solid-like assemblies highly

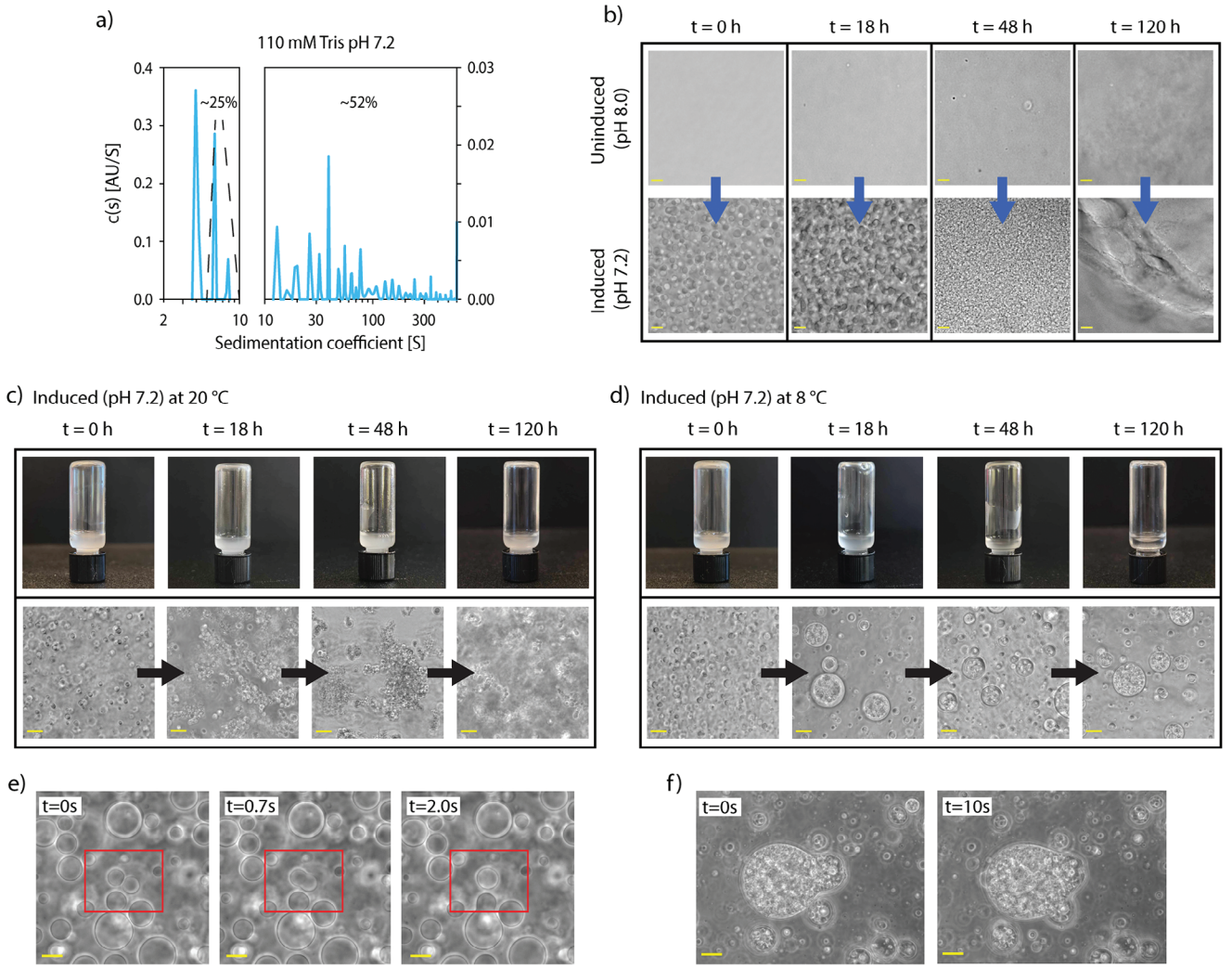

Figure 4. The phase behavior of NT-2Rep-CT at pH 7.2. A) Distribution of sedimentation coefficients for NT-2Rep-CT at 20 g L^{-1} in 110 mM Tris buffer at pH 7.2. B) The outcome of changing pH from 8.0 to pH 7.2 depends strongly on how long the sample had been kept at 20 °C before the pH change was made. Liquid-like condensates were formed if the change was made at t = 0 while a change at t = 120 h resulted in a gel. C) For samples, where the pH change was made at t = 0 and the sample kept at 20 °C, condensates initially formed and changed into irregularly shaped assemblies over time. D) For samples where the pH change was made at t = 0 and the sample was kept at 8 °C, condensates initially formed, and stayed in a liquid form over extended times. E) Liquid-like condensates showing fusion events on the time scale of a few seconds. Snapshots from a sample where LLPS was induced by the pH change from 8.0 to 7.2 at 8 °C at t = 0. F) Condensates after 120 h at pH 7.2 at 8 °C showing slow fusion (on the time scale of tens of seconds). This indicates an increased viscosity.

important to study when dealing with protein material processing, such as spider silk fiber spinning.

2.4. Sample History Strongly Affects the State of the Sample

To obtain a more complete picture of the phase behavior in terms of experimentally observed metastability and dynamic arrest of the different assemblies, we further studied the effect of temperature and the pathway dependence on the appearance of the sample. Pathway dependence is especially important when observing metastable and dynamically arrested states.[67] Starting with an initial sample of 40 g L^{-1} NT-2Rep-CT at pH 8, 20 mM Tris we subjected the samples to a range of temperatures: 8, 20, 30, and 37 °C. The pH was then changed to 7.2 and Tris concentration increased to 110 mM. Condensation was clearly observed at 8 °C (a1), noticeably weaker at 20 °C (a2), and did not occur at 30 °C (a3) and 37 °C (a4) (**Figure 5**). At the latter two temperatures, irregular assemblies were observed instead. Compared to the model diagram in Figure 1, these observations suggest that the points for 8 and 20 °C are now below the binodal and for 30 and 37 °C above the binodal.

At t = 20 min, the temperature of all samples was set to 8 °C. For the samples at temperatures initially higher than 20 °C (b3 and b4), liquid-like condensates were observed together with the irregularly shaped assemblies. The condensates were however smaller than those in samples which had been at lower temperatures. At t = 30 min, we elevated temperatures to 20 °C for the

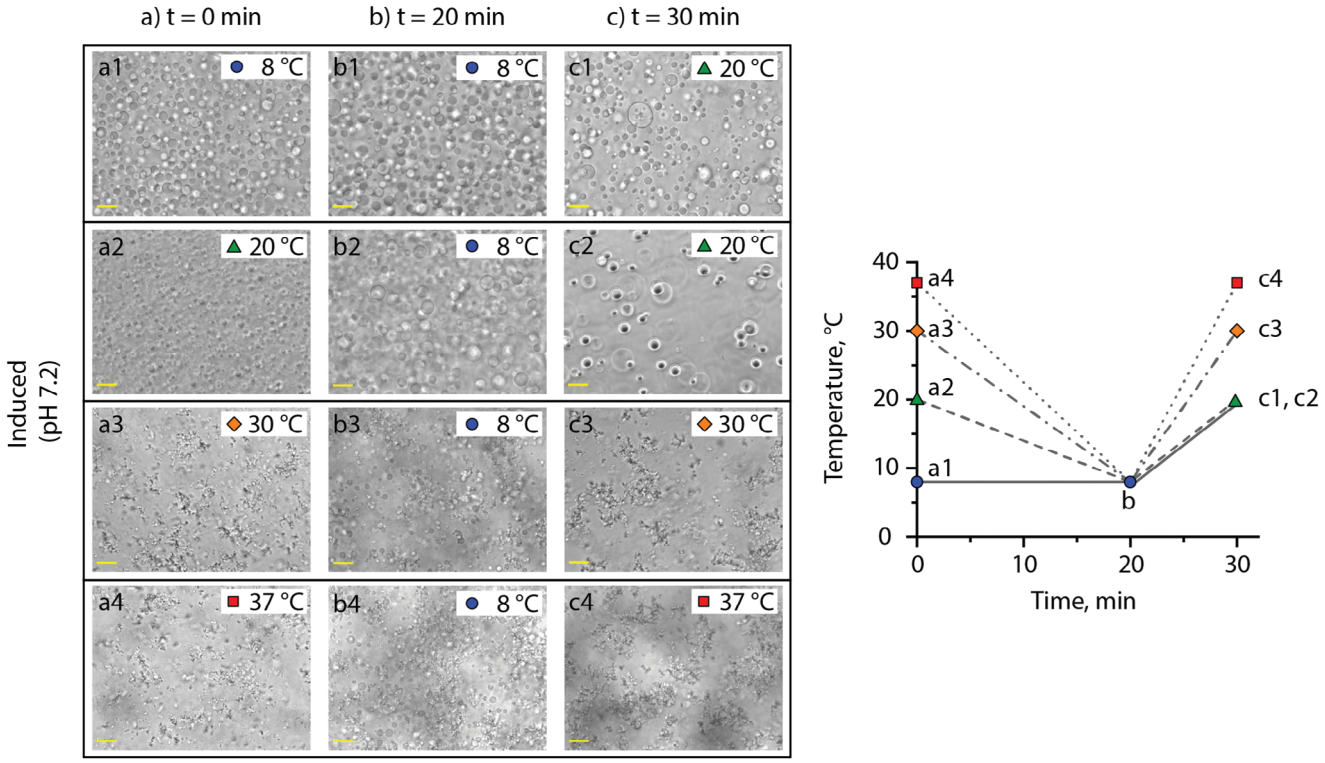

Figure 5. NT-2Rep-CT is induced at different temperatures (column a) and brought to the same thermodynamic state point (column b) leading to different observations based on the state at induction. The temperature of the samples was then elevated again (column c) resulting in shape differences in the persisting coacervates (c1 and c2) and showing the reversibility of NT-2Rep-CT LLPS (c3 and c4). Scale bar 20 µm. The schematic plot illustrates the temperature time-dependency of the sample in each panel.

sample originally at 8 °C (c1) and for the samples originally at 20, 30, and 37 °C back to their original temperatures (c2, c3, and c4). The condensates in c3 and c4 disappeared while condensates in c1 and c2 remained liquid and increased in size with time. The results show that liquid-like condensates were highly reversible with temperature while the irregular assemblies were not readily reversible. This suggests that the irregular assemblies are dynamically arrested clusters or that they are thermodynamically stable with respect to liquid–liquid coexistence. Furthermore, the observations suggest that in the experimental timescale, the liquid-like condensates are reversible in their formation/dissolution and do not become dynamically arrested. Altogether, the metastable binodal for the NT-2Rep-CT appears to be between 20 and 30 °C (20 g L^{-1}, 110 mM Tris, pH7.2) based on these observations.

We next studied the time evolution of NT-2Rep-CT at 20 g L^{-1} for a more extended time. Samples were originally at 8 °C (a1), 20 °C (a2), 30 °C (a3), and 37 °C (a4) when the pH was altered from 8 to 7.2 (**Figure 6**). Similar to the above, arrested clusters were observed at the two higher temperatures. We then lowered the temperature to 8 °C for all samples. In samples originally at 30 °C (b3) and 37 °C (b4) condensates formed, but arrested clusters also remained. There was a noticeable effect of sample history on the growth rate of condensates. The samples originally at 30 and 37 °C showed a faster initial growth of some condensates. All samples showed the evolution of liquid-like condensate droplets toward irregular shapes over time and forming at ≈48 h. These irregular condensates did not fuse nor grow, indicating that they were gel-like. The observations imply that the dynamic arrest line crosses the binodal at these temperatures (see **Figure 7**) and the experimental timescale (48 h) is long enough to observe dynamic arrest.

3. Conclusion

In this work, we have reported on an extensive experimental characterization effort to probe the temporal evolution of NT-2Rep-CT solutions over a wide range of temperatures, solution pH conditions, and protein concentrations. We have observed simple uniform solutions in dilute systems, the presence of metastable liquid–liquid coexistence, and the emergence of irreversible aggregates at higher concentrations. Perhaps most importantly, our experiments have highlighted the critical role of aging on the processing path dependence of mini-spidroin solutions. Based on our experimental observations, a minimalist mini-spidroin phase diagram inspired by colloidal/globular protein systems can be constructed (Figure 7). It is characterized by a solubility line, metastable liquid–liquid coexistence, and a region at high protein concentrations associated with the emergence of irreversible solid/gel aggregates. Upon aging, a system initially located to the right of the solubility line will eventually enter the region associated with irreversible aggregates as indicated by the horizontal squiggly lines in the phase diagram. Quenches in pH or temperature can be represented as vertical lines, and if the quenches occur on time scales faster compared to aging, the system may

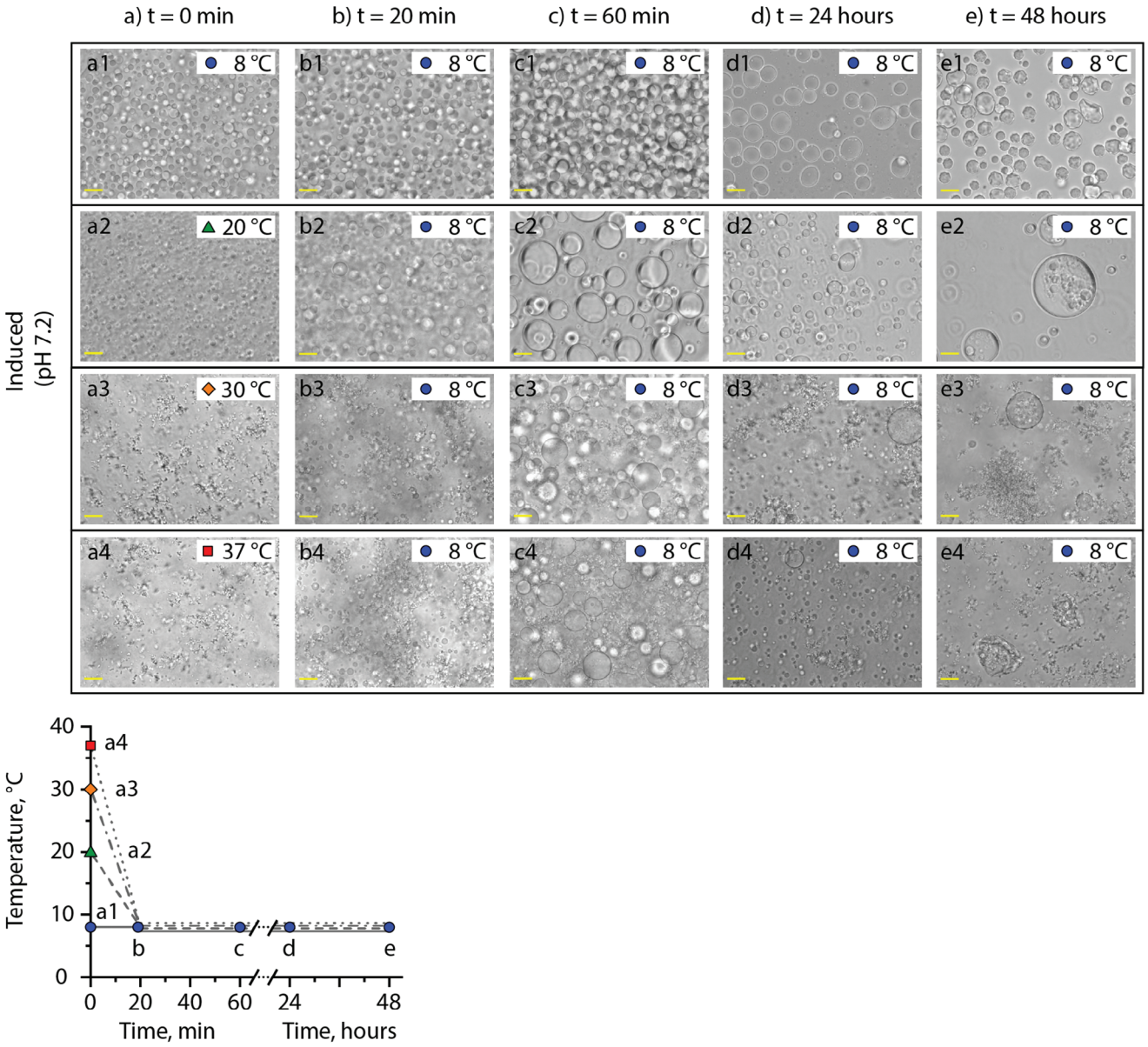

Figure 6. Time evolution of NT-2Rep-CT after phase separation is induced at different temperatures and phase-separated samples are brought down to the same temperature (8 °C) and kept at that temperature for 48 h. Scale bar 20 µm. The schematic plot illustrates the temperature of the sample in each panel at the given time points.

display apparently reversible behavior upon repeated cycling across the metastable binodal line, resulting in the formation and dissolution of condensates; at sufficiently late times, however, the system will enter the irreversible aggregate region. Importantly, subjecting the system to different aging and quench protocols with the same thermodynamic end variables (pH and temperature) will result in widely varying end morphologies as different processing pathways enter the irreversible aggregate regime at different points in the phase diagram. In this work, we used zero-time as the starting point for the study of time-dependent behavior. However, the sample had of course a history prior to this zero-time that could affect the outcomes of the experiments. The zero-time was selected to be the same as used in other studies on the mini-spidroin, for ease of comparison and because no adverse behavior such as precipitation was observed by this procedure.[68] We also note that the sample at the zero-point allowed a wide range of phase behaviors—including dilution to the solubility line—which indicates that the history of the sample did not lead to restriction of available assembly states.

Several recent works have reported on the metastability of LLPS and consequent aging of IDR-containing protein solutions.[40,69,70] These systems are highly complex and rational approaches to understanding their behavior are often missing. Efforts have been made to construct unified frameworks, for example, for amyloid self-assembly[33] and extensive literature exists on globular protein phase transitions.[28,31] However,

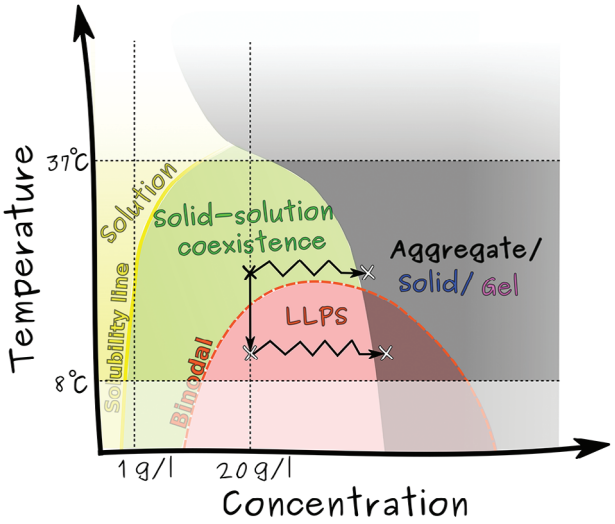

Figure 7. A schematic showing the equilibrium (e.g., solution at 20 °C 0.01 g L^{-1}), metastable (e.g., solution at 20 °C and 5 g L^{-1} and liquid–liquid coexistence in all state points), and arrested states (aggregate/solid/gel at 8–37 °C and 20 g L^{-1}) observed in the experiments of NT-2Rep-CT solutions in the temperature range of 8–37 °C and concentration range of 0.01–40 g L^{-1}. The grey region approximately represents where irreversible solid-like states were observed in the experiments. The horizontal squiggly lines represent the evolution of the sample toward such arrested states during aging, while the solid vertical line corresponds to quenches in pH or temperature.

complete phase diagrams of multidomain proteins and IDPs are lacking due to the complex assembly response and time dependency. It is easily overlooked that it is experimentally difficult to identify true equilibrium states due to the presence of long-lived metastable or dynamically arrested intermediate states. Interestingly, a recent study showed that laser pulses affected the aging of condensates of NT-2Rep-CT, possibly suggesting new routes to expose dynamically arrested states.[71] We urge future experimental and industrial designs to add time as an additional dimension in their study and consider the strong likelihood of encountering metastable and arrested states.[68]

Future efforts in developing particle-based coarse-grained[72–78] and atomistic detail simulation models[79–81] will be key in systematically uncovering molecular-level dependencies of the formation of various protein assembly structures and aging in protein solutions. Atomistic models can provide local structure and uncover individual interactions that lead to specific phase responses, but are currently limited by timescales of up to several µs. On the other hand, coarse-grained models can reach much larger time and length scales to uncover assembly structures and phase response, however, the connection to real systems becomes rather tenuous due to simplifying abstractions. Data-based approaches identify the condition and molecular-level dependencies.[82,83] Often a combination of two (or more) approaches is needed.[72,82] Finally, continuum approaches may be employed to further develop thermodynamic and kinetic insights into complex mixtures of protein solutions.[84–88] In our approach, we make use of a generic phase diagram to understand the time evolution of the protein solution. This strategy facilitates rational techniques for designing and applying methods to produce protein-based materials while also offering valuable insight for understanding protein assembly in living systems.

4. Experimental Section

NT-2Rep-CT Expression: The NT-2Rep-CT construct consists of an N-terminal 6xHis-tag, an N-terminal domain sequence and a repetitive domain sequence from a major ampullate spidroin 1 (MaSp1) sequence from *Euprosthenops australis*, and a C-terminal domain from a minor ampullate spidroin (MiSp) sequence from *Araneus ventricosus* (see Supporting Information for detailed sequences). The DNA sequence encoding NT-2Rep-CT was inserted into a pET28a expression vector using golden gate cloning. The DNA sequence of the expression vector was otherwise the same as the commercially available one, except for two BsaI recognition sites added to the multiple cloning sites.

The plasmid containing the NT-2Rep-CT gene was transformed into the BL21-AI *E. coli* strain (Thermo Fischer Scientific) for protein expression. Cell cultures were grown in TB medium (Terrific Broth, Invitrogen) containing 50 µg mL^{-1} kanamycin overnight at 30 °C with 220 RPM shaking. After overnight growth, the culture was diluted 1/100 with the growth medium and incubated in the same conditions until OD_{600} reached a value of 0.6, measured with a BioPhotometer Plus (Eppendorf), after which the temperature was lowered to 20 °C and protein expression was induced with 1 mM IPTG (Isopropyl β-D-1-thiogalactopyranoside) and 0.2% L-arabinose and carried out for 18 h. Expression was carried out in a 500 mL culture volume in 2 L shake flasks. Cells were harvested by centrifugation (3′900 RPM, 4 °C, 10 min) and cell pellets were frozen at −20 °C.

Protein Purification: Frozen cell pellets were thawed and resuspended in 20 mM Tris-HCl buffer pH 8.0 containing 15 mM imidazole. Cells were lysed using a Q500 tip sonicator (Qsonica) with a 1/2″ tip (2 s pulse on, 2 s pulse off, 1 min total at 40% amplitude three times per tube). The cell lysate was centrifuged (14′000 RPM, 4 °C, 20 min) to separate the soluble fraction, which was purified using immobilized metal affinity chromatography (IMAC). The soluble fraction was loaded onto a 5 mL HisTrap FF (GE Healthcare) Ni-NTA column connected to an ÄKTA pure (GE Healthcare) fast protein liquid chromatography (FPLC) system. The target protein was eluted with 20 mM Tris-HCl at pH 8.0 containing 300 mM imidazole. The eluted protein was dialyzed against 20 mM Tris-HCl at pH 8.0 and at 4 °C using SnakeSkin dialysis membrane (Thermo Fischer Scientific) with a 3.5 kDa M_W cut-off.

The purified protein solution was concentrated to 40 mg mL^{-1} using a Vivaspin centrifugal concentrator with a M_W cut-off of 10 kDa (4′000 RPM, 4 °C). The concentration was determined by measuring the absorbance at 280 nm using a spectrophotometer. Aliquots of concentrated stock solution were snap-frozen with liquid nitrogen and stored at −20 °C. For each experiment, a new aliquot was used.

Analytical Ultracentrifugation: Analytical ultracentrifugation sedimentation velocity (SV) experiments were performed using Beckman Coulter Optima analytical ultracentrifuge. The measurements were carried out at 30′000 RPM using an An-60Ti rotor. All measurements were performed at 20 °C and with the use of an absorbance detector. The measuring cells used standard 12 mm thick Epon centerpieces with quartz windows and 3 mm thick titanium centerpieces with sapphire windows at protein concentrations higher than 5 g L^{-1}. Samples were measured over a range of protein concentrations and wavelengths: 0.05–0.1 g L^{-1} (230 nm), 0.675–1.25 g L^{-1} (280 nm), 2.5–20 g L^{-1} (300 nm). The 20 mM Tris pH 8.0 and 110 mM Tris pH 7.2 buffers were used.

Data analysis of obtained sedimentation profiles was performed by Sedfit software using $c(s)$[89] and nonideal $c(s)$[90] analysis models.

Microscopy: Frozen protein stock solutions were thawed and centrifuged to remove aggregates prior to subsequent experiments. The state of the protein solution after thawing and centrifugation was regarded as $t = 0$. The proteins were mixed with the same buffer conditions as described in the previous section. Samples were kept on temperature-controlled blocks for the duration of the experiments. For image analysis, samples were taken and placed on microscope slides and analyzed immediately. Phase contrast images were taken with an Axio Observer Z1 microscope (Carl

Zeiss, Germany) equipped with a 40x magnification objective and an Axiocam 503 camera. Images were processed using the Zeiss ZEN Blue software.

Statistical Analysis: The raw AUC data were analyzed using 100 scans in each experiment and fitted to the c(s) model in sedimentation coefficient range 0–600 S. Positions of dimer peak were specified using a smaller fitting range and higher resolution. Analysis was performed with a floating meniscus and frictional ratio with a starting value of 1.5 f/f0. Maximum entropy regularization with a factor of 0.51, 0.7, and 0.9 was used. The root-mean-square deviation was in the range from 0.002 to 0.006. The percent of the signal corresponding to dimer and high molecular weight assemblies was calculated using the trapezoidal rule. Trend lines for the time evolution of cluster growth were plotted using second-order polynomial fit. Fitting with the classical Freundlich model was used to make a trend line of the clusters/dimers signal ratio as a function of protein concentration. In all other cases, trend lines were plotted using linear fit.

Supporting Information

Supporting Information is available from the Wiley Online Library or from the author.

Acknowledgements

D.F., F.-E.S., and A.L.H. contributed equally to this work. A.L.H. thanks Dr. Max Philipp Holl for stimulating discussions on phase transitions. This work was supported by the Research Council of Finland under project numbers 346111 (M.S.), 364205 (M.S.), 346105 (M.L.), and 364199 (M.L.) through its Centres of Excellence Programme (2022-2029, LIBER), Novo Nordisk Foundation under project no. NNF22OC0074060 (M.S.), NNF22OC0079084 (A.S.), and NNF20OC0061306 (M.L.). The Bioeconomy Infrastructure at Aalto University is acknowledged for providing facilities.

Conflict of Interest

The authors declare no conflict of interest.

Data Availability Statement

The data that support the findings of this study are openly available in Zenodo at https://doi.org/10.5281/zenodo.13365377, reference number 13365377.

Keywords

analytical ultracentrifugation, intrinsically disordered protein, liquid–liquid phase separation, spidroin

Received: June 14, 2024
Revised: August 29, 2024
Published online:

[1] J. Johansson, A. Rising, *ACS Nano* **2021**, *15*, 1952.
[2] T. D. Sutherland, J. H. Young, S. Weisman, C. Y. Hayashi, D. J. Merritt, *Annu. Rev. Entomol.* **2010**, *55*, 171.
[3] S. Keten, Z. Xu, B. Ihle, M. J. Buehler, *Nat. Mater.* **2010**, *9*, 359.
[4] M. Heim, D. Keerl, T. Scheibel, *Angew. Chem., Int. Ed.* **2009**, *48*, 3584.
[5] R. V. Pappu, S. R. Cohen, F. Dar, M. Farag, M. Kar, *Chem. Rev.* **2023**, *123*, 8945.
[6] B. Schmuck, G. Greco, T. B. Pessatti, S. Sonavane, V. Langwallner, T. Arndt, A. Rising, *Adv. Funct. Mater.* **2024**, *34*, 2305040.
[7] G. Askarieh, M. Hedhammar, K. Nordling, A. Saenz, C. Casals, A. Rising, J. Johansson, S. D. Knight, *Nature* **2010**, *465*, 236.
[8] F. Hagn, L. Eisoldt, J. G. Hardy, C. Vendrely, M. Coles, T. Scheibel, H. Kessler, *Nature* **2010**, *465*, 239.
[9] T. Arndt, G. Greco, B. Schmuck, J. Bunz, O. Shilkova, J. Francis, N. M. Pugno, K. Jaudzems, A. Barth, J. Johansson, A. Rising, *Adv. Funct. Mater.* **2022**, *32*, 2200986.
[10] L. Nilebäck, S. Arola, M. Kvick, A. Paananen, M. B. Linder, M. Hedhammar, *Langmuir* **2018**, *34*, 11795.
[11] M. Andersson, Q. Jia, A. Abella, X.-Y. Lee, M. Landreh, P. Purhonen, H. Hebert, M. Tenje, C. V. Robinson, Q. Meng, G. R. Plaza, J. Johansson, A. Rising, *Nat. Chem. Biol.* **2017**, *13*, 262.
[12] B. Schmuck, G. Greco, A. Barth, N. M. Pugno, J. Johansson, A. Rising, *Mater. Today* **2021**, *50*, 16.
[13] T. Arndt, K. Jaudzems, O. Shilkova, J. Francis, M. Johansson, P. R. Laity, C. Sahin, U. Chatterjee, N. Kronqvist, E. Barajas-Ledesma, R. Kumar, G. Chen, R. Strömberg, A. Abelein, M. Langton, M. Landreh, A. Barth, C. Holland, J. Johansson, A. Rising, *Nat. Commun.* **2022**, *13*, 4695.
[14] A. Leppert, G. Chen, D. Lama, C. Sahin, V. Railaite, O. Shilkova, T. Arndt, E. G. Marklund, D. P. Lane, A. Rising, M. Landreh, *Nano Lett.* **2023**, *23*, 5836.
[15] P. Mohammadi, A. S. Aranko, L. Lemetti, Z. Cenev, Q. Zhou, S. Virtanen, C. P. Landowski, M. Penttilä, W. J. Fischer, W. Wagermaier, M. B. Linder, *Commun. Biol.* **2018**, *1*, 86.
[16] T. Välisalmi, H. Bettahar, Q. Zhou, M. B. Linder, *Int. J. Biol. Macromol.* **2023**, *250*, 126161.
[17] Y. Yin, N. Roas-Escalona, M. B. Linder, *Adv. Mater. Interfaces* **2024**, *11*, 2300934.
[18] Y. Shin, C. P. Brangwynne, *Science* **2017**, *357*, eaaf4382.
[19] S. Boeynaems, S. Alberti, N. L. Fawzi, T. Mittag, M. Polymenidou, F. Rousseau, J. Schymkowitz, J. Shorter, B. Wolozin, L. Van Den Bosch, P. Tompa, M. Fuxreiter, *Trends Cell Biol.* **2018**, *28*, 420.
[20] M. J. Harrington, R. Mezzenga, A. Miserez, *Nat. Rev. Bioeng.* **2023**, *2*, 260.
[21] J. H. Waite, *J. Exp. Biol.* **2017**, *220*, 517.
[22] Y. Tan, S. Hoon, P. A. Guerette, W. Wei, A. Ghadban, C. Hao, A. Miserez, J. H. Waite, *Nat. Chem. Biol.* **2015**, *11*, 488.
[23] M. J. Brennan, B. F. Kilbride, J. J. Wilker, J. C. Liu, *Biomaterials* **2017**, *124*, 116.
[24] M. Du, Z. J. Chen, *Science* **2018**, *361*, 704.
[25] A. Klosin, F. Oltsch, T. Harmon, A. Honigmann, F. Jülicher, A. A. Hyman, C. Zechner, *Science* **2020**, *367*, 464.
[26] P. Li, S. Banjade, H.-C. Cheng, S. Kim, B. Chen, L. Guo, M. Llaguno, J. V. Hollingsworth, D. S. King, S. F. Banani, P. S. Russo, Q.-X. Jiang, B. T. Nixon, M. K. Rosen, *Nature* **2012**, *483*, 336.
[27] F. Frottin, F. Schueder, S. Tiwary, R. Gupta, R. Körner, T. Schlichthaerle, J. Cox, R. Jungmann, F. U. Hartl, M. S. Hipp, *Science* **2019**, *365*, 342.
[28] A. Stradner, P. Schurtenberger, *Soft Matter* **2020**, *16*, 307.
[29] S. Alberti, *J. Cell Sci.* **2017**, *130*, 2789.
[30] H.-X. Zhou, V. Nguemaha, K. Mazarakos, S. Qin, *Trends Biochem. Sci.* **2018**, *43*, 499.
[31] J. J. McManus, P. Charbonneau, E. Zaccarelli, N. Asherie, *Curr. Opin. Colloid Interface Sci.* **2016**, *22*, 73.
[32] C. P. Brangwynne, P. Tompa, R. V. Pappu, *Nat. Phys.* **2015**, *11*, 899.
[33] T. C. T. Michaels, D. Qian, A. Šarić, M. Vendruscolo, S. Linse, T. P. J. Knowles, *Nat. Rev. Phys.* **2023**, *5*, 379.
[34] Y. Lin, D. S. W. Protter, M. K. Rosen, R. Parker, *Mol. Cell* **2015**, *60*, 208.

[35] A. Patel, H. O. Lee, L. Jawerth, S. Maharana, M. Jahnel, M. Y. Hein, S. Stoynov, J. Mahamid, S. Saha, T. M. Franzmann, A. Pozniakovski, I. Poser, N. Maghelli, L. A. Royer, M. Weigert, E. W. Myers, S. Grill, D. Drechsel, A. A. Hyman, S. Alberti, *Cell* **2015**, *162*, 1066.
[36] A. Mahapatra, R. W. Newberry, *Protein Sci.* **2024**, *33*, e4951.
[37] S. Elbaum-Garfinkle, Y. Kim, K. Szczepaniak, C. C.-H. Chen, C. R. Eckmann, S. Myong, C. P. Brangwynne, *Proc. Natl. Acad. Sci.* **2015**, *112*, 7189.
[38] M.-T. Wei, S. Elbaum-Garfinkle, A. S. Holehouse, C. C.-H. Chen, M. Feric, C. B. Arnold, R. D. Priestley, R. V. Pappu, C. P. Brangwynne, *Nat. Chem.* **2017**, *9*, 1118.
[39] N. M. Kanaan, C. Hamel, T. Grabinski, B. Combs, *Nat. Commun.* **2020**, *11*, 2809.
[40] T. Das, F. Zaidi, M. Farag, K. M. Ruff, J. Messing, J. P. Taylor, R. V. Pappu, T. Mittag, *bioRxiv* **2024**, https://doi.org/10.1101/2024.02.28.582569.
[41] N. Asherie, A. Lomakin, G. B. Benedek, *Phys. Rev. Lett.* **1996**, *77*, 4832.
[42] M. L. Broide, C. R. Berland, J. Pande, O. O. Ogun, G. B. Benedek, *Proc. Natl. Acad. Sci* **1991**, *88*, 5660.
[43] C. R. Berland, G. M. Thurston, M. Kondo, M. L. Broide, J. Pande, O. Ogun, G. B. Benedek, *Proc. Natl. Acad. Sci* **1992**, *89*, 1214.
[44] J. A. Thomson, P. Schurtenberger, G. M. Thurston, G. B. Benedek, *Proc. Natl. Acad. Sci* **1987**, *84*, 7079.
[45] V. G. Taratuta, A. Holschbach, G. M. Thurston, D. Blankschtein, G. B. Benedek, *J. Phys. Chem.* **1990**, *94*, 2140.
[46] R. Maier, G. Zocher, A. Sauter, S. D.a Vela, O. Matsarskaia, R. Schweins, M. Sztucki, F. Zhang, T. Stehle, F. Schreiber, *Cryst. Growth Des.* **2020**, *20*, 7951.
[47] M. Shah, O. Galkin, P. G. Vekilov, *J. Chem. Phys.* **2004**, *121*, 7505.
[48] M. Muschol, F. Rosenberger, *J. Chem. Phys.* **1997**, *107*, 1953.
[49] S. M. Ilett, A. Orrock, W. C. K. Poon, P. N. Pusey, *Phys. Rev. E* **1995**, *51*, 1344.
[50] M. H. J. Hagen, D. Frenkel, *J. Chem. Phys.* **1994**, *101*, 4093.
[51] A. D. Malay, T. Suzuki, T. Katashima, N. Kono, K. Arakawa, K. Numata, *Sci. Adv.* **2020**, *6*, eabb6030.
[52] J. Feng, B. Gabryelczyk, I. Tunn, E. Osmekhina, M. B. Linder, *ACS Synth. Biol.* **2023**, *12*, 3050.
[53] M. A. Blanco, *mAbs* **2022**, *14*, 2044744.
[54] M. Landreh, M. Andersson, E. G. Marklund, Q. Jia, Q. Meng, J. Johansson, C. V. Robinson, A. Rising, *Chem. Commun.* **2017**, *53*, 3319.
[55] O. Gliko, W. Pan, P. Katsonis, N. Neumaier, O. Galkin, S. Weinkauf, P. G. Vekilov, *J. Phys. Chem. B* **2007**, *111*, 3106.
[56] N. Chen, C. Chassenieux, T. Nicolai, *Food Hydrocoll.* **2018**, *77*, 66.
[57] N. Chen, M. Zhao, C. Chassenieux, T. Nicolai, *Food Hydrocoll.* **2016**, *61*, 740.
[58] M. Wolz, U. Kulozik, *Int. Dairy J.* **2015**, *49*, 95.
[59] D.-H. Tsai, L. F. Pease III, R. A. Zangmeister, M. J. Tarlov, M. R. Zachariah, *Langmuir* **2009**, *25*, 140.
[60] P. G. Vekilov, *Nanoscale* **2010**, *2*, 2346.
[61] P. R. ten Wolde, D. Frenkel, *Science* **1997**, *277*, 1975.
[62] D. Erdemir, A. Y. Lee, A. S. Myerson, *Acc. Chem. Res.* **2009**, *42*, 621.
[63] A. Jawor-Baczynska, B. D. Moore, H. S. Lee, A. V. McCormick, J. Sefcik, *Faraday Discuss.* **2014**, *167*, 425.
[64] D. Gebauer, A. Völkel, H. Cölfen, *Science* **2008**, *322*, 1819.
[65] D. Gebauer, M. Kellermeier, J. D. Gale, L. Bergström, H. Cölfen, *Chem. Soc. Rev.* **2014**, *43*, 2348.
[66] O. Galkin, W. Pan, L. Filobelo, R. E. Hirsch, R. L. Nagel, P. G. Vekilov, *Biophys. J.* **2007**, *93*, 902.
[67] V. J. Anderson, H. N. W. Lekkerkerker, *Nature* **2002**, *416*, 811.
[68] B. Schmuck, G. Greco, F. G. Bäcklund, N. M. Pugno, J. Johansson, A. Rising, *Commun. Mater.* **2022**, *3*, 83.
[69] L. Jawerth, E. Fischer-Friedrich, S. Saha, J. Wang, T. Franzmann, X. Zhang, J. Sachweh, M. Ruer, M. Ijavi, S. Saha, J. Mahamid, A. A. Hyman, F. Jülicher, *Science* **2020**, *370*, 1317.
[70] I. Alshareedah, W. M. Borcherds, S. R. Cohen, A. Singh, A. E. Posey, M. Farag, A. Bremer, G. W. Strout, D. T. Tomares, R. V. Pappu, T. Mittag, P. R. Banerjee, *Nat. Phys.* **2024**, *20*, 1482.
[71] A. Leppert, J. Feng, V. Railaite, T. Bohn Pessatti, C. P. Cerrato, C. Mörman, H. Osterholz, D. P. Lane, F. R. N. C. Maia, M. B. Linder, A. Rising, M. Landreh, *J. Am. Chem. Soc.* **2024**, *146*, 19555.
[72] A. Garaizar, J. R. Espinosa, J. A. Joseph, G. Krainer, Y. Shen, T. P. J. Knowles, R. Collepardo-Guevara, *Proc. Natl. Acad. Sci* **2022**, *119*, 2119800119.
[73] G. L. Dignon, W. Zheng, Y. C. Kim, R. B. Best, J. Mittal, *PLoS Comput. Biol.* **2018**, *14*, e1005941.
[74] S. R. Cohen, I. Alshareedah, W. M. Borcherds, M. Farag, T. Mittag, P. R. Banerjee, R. V. Pappu, *Biophys. J.* **2023**, *122*, 206a.
[75] F. Dar, S. R. Cohen, D. M. Mitrea, A. H. Phillips, G. Nagy, W. C. Leite, C. B. Stanley, J.-M. Choi, R. W. Kriwacki, R. V. Pappu, *Nat. Commun.* **2024**, *15*, 3413.
[76] L. Lemetti, A. Scacchi, Y. Yin, M. Shen, M. B. Linder, M. Sammalkorpi, A. S. Aranko, *Biomacromolecules* **2022**, *23*, 3142.
[77] P. Mohanty, U. Kapoor, D. Sundaravadivelu Devarajan, T. M. Phan, A. Rizuan, J. Mittal, *Biochemistry* **2022**, *61*, 2443.
[78] J.-M. Choi, F. Dar, R. V. Pappu, *PLoS Comput. Biol.* **2019**, *15*, e1007028.
[79] S. Rekhi, C. G. Garcia, M. Barai, A. Rizuan, B. S. Schuster, K. L. Kiick, J. Mittal, *Nat. Chem.* **2024**, *16*, 1113.
[80] P. Batys, D. Fedorov, P. Mohammadi, L. Lemetti, M. B. Linder, M. Sammalkorpi, *Biomacromolecules* **2021**, *22*, 690.
[81] S. Blazquez, I. Sanchez-Burgos, J. Ramirez, T. Higginbotham, M. M. Conde, R. Collepardo-Guevara, A. R. Tejedor, J. R. Espinosa, *Adv. Sci.* **2023**, *10*, 2207742.
[82] K. L. Saar, D. Qian, L. L. Good, A. S. Morgunov, R. Collepardo-Guevara, R. B. Best, T. P. J. Knowles, *Chem. Rev.* **2023**, *123*, 8988.
[83] S. Navarro, S. Ventura, *Curr. Opin. Struct. Biol.* **2022**, *73*, 102343.
[84] A. Scacchi, M. Vuorte, M. Sammalkorpi, *Adv. Phys. X* **2024**, *9*, 2358196.
[85] D. López Barreiro, J. Yeo, A. Tarakanova, F. J. Martin-Martinez, M. J. Buehler, *Macromol. Biosci.* **2019**, *19*, 1800253.
[86] R. Zhang, S. Mao, M. P. Haataja, *J. Chem. Phys.* **2024**, *160*, 244903.
[87] J. Berry, C. P. Brangwynne, M. Haataja, *Rep. Prog. Phys.* **2018**, *81*, 046601.
[88] S. Mao, D. Kuldinow, M. P. Haataja, A. Košmrlj, *Soft Matter* **2019**, *15*, 1297.
[89] P. Schuck, M. A. Perugini, N. R. Gonzales, G. J. Howlett, D. Schubert, *Biophys. J.* **2002**, *82*, 1096.
[90] S. K. Chaturvedi, J. Ma, P. H. Brown, H. Zhao, P. Schuck, *Nat. Commun.* **2018**, *9*, 4415.